Workshop hypersonique d'Antibes, avril 1991.

Computation of Hypersonic Flows with a Fully Coupled Implicit Solver and an Extension of the CVDV Model for Thermochemical Relaxation

G. MEHLMAN[†‡], F. THIVET [*], S. CANDEL[*] and F. DUBOIS[‡]

† Centre de Mathématiques Appliquées
Ecole Polytechnique
91128 Palaiseau Cedex, France

* Laboratoire E.M2.C., C.N.R.S.
Ecole Centrale de Paris
92295 Châtenay-Malabry Cedex, France

‡ Aérospatiale, Division Systèmes Stratégiques et Spatiaux
Département de Mathématiques Appliquées
78133 Les Mureaux, France

Introduction

Quasi-1D and 2D axisymmetric results concerning test case VIII.2 are presented.

The 2D Euler equations for a mixture of fluids in thermochemical nonequilibrium are solved by a time stepping procedure, which is described in Section 1. The unknowns considered are the complete set of conservative variables ρ_i, ρu, ρv, ρe, and $\rho_i e_i^{vib}$ which denote respectively the partial densities, the momentum in the x and y directions, the total energy and the vibrational energies of each species. Solutions are computed with a fully coupled approach : the source term due to chemical and vibrational relaxation is dicretized with a linearized backward Euler scheme during the same time interval as the flux terms which are treated with an approximate Riemann solver for multicomponent flows [1].

In Section 2, the physical modelization and its implementation are presented. In particular, a thorough vibrational relaxation model is outlined.

In Section 3, we will focus on our approach to the quasi-1D problem. The originality of this approach lies in the geometrical modelization, which allows us to obtain the solution by using the same 2D code as for the axisymmetric problem.

Numerical results are presented in Section 4.

*Tel. 47 02 70 56, Fax. 47 02 80 35

1 Presentation of the Solver

An Unstructured Approach

The code is based on the MUSCL scheme proposed initially by Van Leer [2] and the use of finite element type unstructured meshes. The computational domain is divided into finite volumes K (non regular quadrangles) which satisfy the usual restrictions associated with finite element meshes. The finite volume formulation requires the evaluation of a numerical flux at each cell interface. These numerical fluxes are computed according to the second order accurate MUSCL approach (Van Leer [2]). Since the mesh is unstructured, the evaluation of the gradients of the conservative variables is carried out in a centered manner through a finite element approach which is exact for quadratic polynomials in x and y. The nonlinear extrapolation of the field ϕ towards the edges of the cell K generalizes the procedure introduced by Van Leer [3]. The field $\phi(K,f)$ at the cell edge f is extrapolated between the centers $x(K)$ of the cell K and $x(f)$ of the interface according to :

$$\phi(K,f) = \phi(K) + \alpha(K,\phi) \cdot \nabla\phi(K) \cdot (x(f) - x(K)) \,,$$

where $\phi(K)$ is the value of the field ϕ at the center of the cell and $\alpha(K,\phi)$ is a parameter (Dubois and Michaux [4]) chosen as close to 1 as possible in order to satisfy the following monotonicity condition :

$$\begin{array}{lll} \max\limits_{\substack{L\, neighboring\, K \\ \phi(L) \le \phi(K)}} (\phi(L) - \phi(K)) & \le 2\,(\phi(K,f) - \phi(K)) \le & \min\limits_{\substack{L\, neighboring\, K \\ \phi(L) \ge \phi(K)}} (\phi(L) - \phi(K)) \end{array} \quad , \forall f \in K$$

This limitation, which is a truly multidimensional version of the minmod limiter, is applied in such a way that the local proportions of atoms are preserved.

The Approximate Riemann Solver

At each interface f, the exact solution of the Riemann problem between the two adjacent states is replaced by an approximate solution. The rarefaction waves present in the exact solution are replaced by shock waves, so that the problem now consists in solving the intersection of the entire shock curves. Since only the shock curves are required, this approach is more efficient than Godunov's scheme [5]. This idea was initially proposed by Collela and Glaz [6] for real gases.

This approximate Riemann solver preserves the positivity of the mass fractions as well as the local proportions of atoms. Moreover, this approach defines a Roe-type linearization [7] and its numerical complexity does not depend on the number of species considered (see [1] for details concerning these properties).

Boundary Conditions

The different boundary conditions present in the numerical problem have been derived by Dubois [8] for Osher's scheme. They have been adapted to our approximate Riemann solver which is based on a shock curve decomposition [1]. These conditions are treated weakly by introducing an adequate external state in a Riemann problem at the boundary.

- At the wall, the external state consists in the mirror state (same thermodynamical state, opposite normal velocity).
- At the inlet, the external state consists in the unique state which can be connected by a shock and a contact surface to the internal state and whose entropy and enthalpy are equal to those in the reservoir.
- At the outlet (which is supersonic when convergence is reached in this problem), two cases must be distinguished. If the internal state is subsonic, the external state is the unique sonic point which can be connected by a shock wave. Otherwise, a simple extrapolation is performed.

Implicit Scheme

This scheme is made implicit by evaluating only the first order terms in the fluxes defined previously at the following time-step. This evaluation is obtained by linearizing around the current time-step an extension of Roe's approximate Riemann solver for multicomponent flows [9]. The implicit step is solved by Jacobi iterations applied to the block pentadiagonal matrix resulting from the unstructured quadrangular mesh.

2 Physical Aspects of the Problem

Vibrational Non-Equilibrium Model

Since chemical relaxation is prescribed, only the vibrational model is described here. Kinetic theory is applied to a mixture of monoatomic and diatomic molecules in order to derive a rigorous macroscopic equation corresponding to the relaxation of vibrational energy :

$$\frac{\partial \rho_i e_i^{vib}}{\partial t} + \nabla . \left(\rho_i e_i^{vib} \mathrm{v} \right)$$

$$= \frac{\rho_i \overline{e_i^{vib}} - \rho_i e_i^{vib}}{\tau_i^{vt}}$$

$$+ \sum_{j=1}^{ns} \frac{X_j}{\tau_{ij}^{vv}} \left\{ \frac{\tau_{ij} \rho_j e_j^{vib}}{\rho_j \overline{e_j^{vib}}} \left(\rho_i \overline{e_i^{vib}} - \rho_i e_i^{vib} \right) - \rho_i e_i^{vib} \left(1 - \frac{\rho_j e_j^{vib}}{\rho_j \overline{e_j^{vib}}} \right) \right\}$$

$$- \frac{\rho_i \widetilde{e_i^{vib}} - \rho_i e_i^{vib}}{Y_i} \left(\frac{dY_i}{dt} \right)_f + \frac{\rho_i g_i^{vib} - \rho_i e_i^{vib}}{Y_i} \left(\frac{dY_i}{dt} \right)_r$$

where

$$\overline{e_i^{vib}} = e_i^{vib}(T) \, ,$$

$$\tau_{ij} = \frac{1 - \exp\left(-\Theta_i^v / T\right)}{1 - \exp\left(-\Theta_j^v / T\right)} \, ,$$

and

$$\frac{1}{\tau_i^{vt}} = \sum_{j=1}^{ns} \frac{X_j}{\tau_{ij}^{vt}} \, .$$

The first term on the right hand side of the relaxation equation is the classical Landau-Teller term. The second term describes the Vibration-Vibration exchanges between diatomic molecules in the mixture. In these expressions τ_{ij}^{vt} and τ_{ij}^{vv} denote respectively the relaxation times for Vibration-Translation and Vibration-Vibration exchanges between molecules M_i and M_j. These elementary times are determined through an extension of the SSH theory [10] [11] to high temperatures.

The last term of the relaxation equation accounts for the influence of chemistry on vibrational relaxation. The quantities $\widetilde{e_k^{vib}}$ and g_k^{vib} represent respectively the average vibrational energy lost by dissociation or gained by recombination [12].

Finally, in a mixture in vibrational non-equilibrium, the chemical reaction rate constants are in turn affected. These constants are related to their values at thermal equilibrium by the relations :

$$K_{neq}^{frd} = V(T, T_i^{vib}) K_{eq}^{frd}(T) \quad \text{and} \quad K_{neq}^{rev} = K_{eq}^{rev}(T)$$

for the dissociation of molecule M_i . A detailed expression of the vibrational factor $V(T, T_k^{vib})$ as well as equivalent relations for exchange reactions may be found in [13] [11].

Implementation of Real Gas Effects

The thermodynamic properties of the species and the source terms which appear in the governing equations are computed in a separate package [14] in such a way that the computer code is completely independent of the physical and chemical modeling. This package has been extended to take into account the vibrational nonequilibrium and its coupling with the chemical kinetics. It can be used for any reaction mechanism describing a gaseous mixture and in particular Park's model [15] for air.

Since the chemical and vibrational source terms are discretized with a linearized backward Euler temporal scheme, their jacobians are required at each time step and are evaluated numerically. This makes the treatment of the source terms compatible with different modelizations and becomes necessary when considering sophisticated models of vibrational nonequilibrium where these jacobians can no longer be determined algebraically.

3 Geometrical Modelization of the Nozzle

A Quasi-1D Approach with a 2D Solver

The exact geometry of test case VIII.2 is a conical axisymmetric convergent and divergent nozzle of respective half-cone angles $\theta = 45°$ and $\Theta = 10°$. The throat is simply defined as the intersection of these cones. Its radius is of $r_o = 0.003$ m and the length of the divergent part is $L = 1.13$ m (Fig.1).

In the quasi-1D approach, the flow field depends only on the variation of the nozzle's section along the x-axis. Consequently, the previously defined nozzle and any nozzle of rectangular section verifying the same section law admit the same quasi-1D solution. In particular, we consider rectangular sections of dimensions $2y(x)$ and l such that :

$$2\,y(x)\,l \;=\; \pi r(x)^2\,, \tag{1}$$

where l is a constant and $r(x) = r_o + x \cdot \tan\Theta$ (Fig.1).

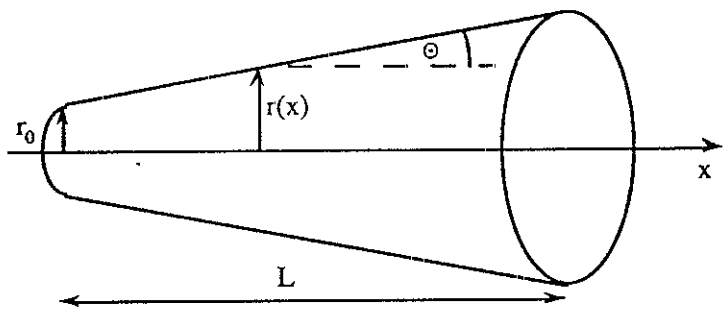

Figure 1: Axisymmetric Nozzle.

In agreement with the quasi-1D approximation, this domain is discretized by cells whose interfaces are perpendicular to the x-axis and cover the entire section (Fig.2). Since the fluxes on the transverse walls parallel to the x-axis cancel out, the quasi-1D solution can be obtained by a 2D computation in the $x - y$ plane. This domain will be referred to as the computational domain.

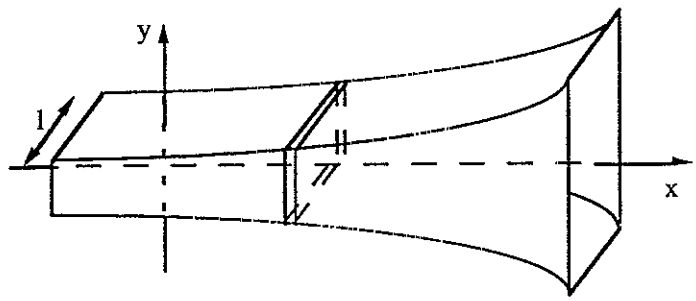

Figure 2: Equivalent Nozzle in the Quasi-1D Approximation.

In order to maintain the quasi-1D flow assumption, the normal Mach number M_n at the walls of the computational domain must be limited to ensure that no cavitation occurs in the Riemann problem along this boundary. A perfect gas estimate yields $M_n = 1.5$. Let $\alpha(x)$ denote the angle of the walls with the x-axis. Since we expect a maximum Mach number of $M_{out} = 11$ at the outlet [16], the following sufficient condition is required (Fig.3) :

$$\alpha(L) \leq \alpha_{max} \text{ , where } \alpha_{max} = \arcsin\left(\frac{M_n}{M_{out}}\right) .$$

Furthermore, consistency with the quasi-1D approximation requires that α_{max} verify the small angle hypothesis.

From Eq.1 we deduce

$$\tan\alpha(x) = \frac{dy}{dx} = \frac{\pi}{l} \tan\Theta \left(r_o + x \cdot \tan\Theta\right) ,$$

which implies

$$l \geq l_{min} \text{ , where } l_{min} = \pi \frac{\tan\Theta}{\tan\alpha_{max}} \left(r_o + L \cdot \tan\Theta\right) .$$

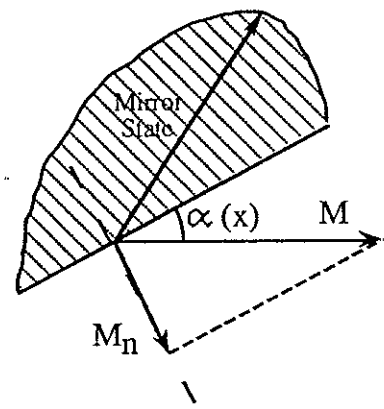

Figure 3: Constraint on $\alpha(x)$.

Since $l_{min} = 0.81$ m , the value $l = 1.00$ m has been chosen.

The divergent part of the nozzle is discretized by 300 cells whose interfaces are exponentially distributed along the x-axis in such a way that the step is of $5. \ 10^{-4}$ m at the throat and of $1.25 \ 10^{-2}$ m at the outlet. Similarly, the convergent part is discretized by 20 cells such that the step is of $5.4 \ 10^{-4}$ m at the throat and of $4. \ 10^{-3}$ m at the inlet.

Meshes for the Axisymmetric Approach

The computational domain consits in this case of half of a symmetry plane of the nozzle. In contrast with the geometry used for the quasi-1D problem, a smooth throat shape has been adopted according to the later technical appendix. Solutions have been obtained on two different meshes :

- a crude mesh with 60 cells in the axial direction and 10 cells in the radial direction.
- a fine mesh with twice as many cells in each direction (120×20).

For both meshes, the cell interfaces are exponentially distributed along the x-axis in such a way that the step is of respectively $2.6 \, 10^{-3}$ m and $6.6 \, 10^{-4}$ m at the throat and of $6.0 \, 10^{-2}$ m and $4.6 \, 10^{-2}$ m at the outlet. The convergent part of the nozzle is discretized similarly. The curved part of the throat region is discretized uniformly in the axial direction with respectively 2 and 8 cells.

4 Results

Test case VIII.2 has been considered with Park's model [15] for chemical relaxation and the vibrational nonequilibrium model described previously for the diatomic species O_2 and N_2. Since the relaxation times of NO are very small [17], this species has been assumed to be at thermodynamic equilibrium. Moreover, since the chemical kinetics model is not valid at low temperatures, chemistry has been frozen below 1000 K.

Numerical performances. The ratio of the cells for the quasi-1D mesh described above is of 2315, which is relatively severe. From the start, second order accuracy was maintained for all computations. A frozen solution, initialized with the reservoir conditions at rest, was first computed. The supersonic outlet boundary condition in this case acted as if the reservoir were emptying. The CFL during this approach phase was typically of the order of 5.0 . At this point, the outlet temperature of 154 K was to low to trigger vibrational non-equilibrium with our model. Therefore, during 4000 iterations at a CFL of 5.0 , only chemical relaxation was activated. This brought the outlet temperature up to 400 K. The complete non-equilibrium model was then introduced and 3000 iterations at a CFL of 5.0, followed by 5000 iterations at a CFL of 50.0 were performed. There was no noticeable change in the solution during the last 2000 iterations. If we consider the logarithm of the normalized L_2 residual norm starting from the frozen solution, more than four orders of magnitude were lost (Fig.18).

This solution serves as an initial flowfield for the axisymmetric computation. Again, on both the crude and the fine meshes, the spatially second order accurate scheme is used from the start. Vibrational equilibrium is imposed during the early stages of the computations. On the crude mesh, the L_2 residual norm drops by almost five orders after 3000 iterations at a CFL of 3.0. Convergence was reached on the fine mesh after 1200 iterations starting from the crude mesh solution. The CPU performance is of aproximately 10 ms per iteration and per mesh cell on an IBM 3090 scalar computer.

Comparison of the quasi-1D and 2D solutions. Iso-value contours of the 2D solution on the refined grid are presented in Figures 1 to 8. The quasi-1D plots are compared to the profiles along the nozzle axis of the axisymmetric solutions for both meshes in Figures 9 to 16. It appears clearly that the crude mesh is not fine enough to obtain a satisfactory solution. Important discrepancies are particularly visible on the entropy and mass flow rate curves (Fig.15,16). On the other hand, the refinement of the 2D grid leads to profiles along the x-axis which are very close to the quasi-1D results. In fact, the iso-value contours show that the flow is almost conical. The angular geometry of the throat in the quasi-1D case induces perturbations of the mass flow rate only.

Physical features of the flowfield. The frozen Mach number reaches the value of 11.93 at the outlet. The mass fractions of diatomic molecules freeze within a distance of 10 cm from the throat. The mass flow rate is of respectively 1.920 Kg/s $\pm$ 0.1 % and 1.940 Kg/s $\pm$ 0.05 % in the quasi-1D and 2D solutions.

The vibrational temperature of N_2 freezes at the relatively low level of 2070 K. Oxygen, which has a smaller relaxation time than does Nitrogen, freezes further downstream and drops to 827 K at the outlet while the transrotational temperature is of 334 K at this point. Note that in our model, collisions between diatomic molecules and open shell atoms are taken into account. These collisions are much more efficient than the collisions between diatomic molecules. In the region of the throat vibrational equilibrium is then maintained thanks to the relatively high mass fractions of monoatomic species (Fig.12,13).

References

[1] G.M. MEHLMAN, An Approximate Riemann Solver for Fluid Systems Based on a Shock Curve Decomposition, Proceedings of the 3rd International Conference on Hyperbolic Problems, (1990).

[2] B. VAN LEER, Towards the Ultimate Conservative Scheme V. A Second Order Sequel to Godunov's Method, *J. Comp. Phys.*, **32**, pp.101-136, (1979).

[3] VAN LEER B., Towards the Ultimate Conservative Scheme IV. A New Approach to Numerical Convection, *J. Comp. Phys.*, **23**, pp.276-299, (1977).

[4] F. DUBOIS, O. MICHAUX, Solution of the Euler Equations Around a Double Ellipsoidal Shape Using Unstructured Meshes and Including Real Gas Effects, Proceedings of the INRIA-GAMNI Hypersonic Workshop, Antibes, France, 22-25 January 1990.

[5] S.K. GODUNOV, A Difference Scheme for Numerical Computation of Discontinuous Solutions of Equations of Fluid Dynamics, *Math. Sbornik,* **47**, pp.271-290, (1959) (in Russian).

[6] P. COLLELA, H.M. GLAZ, Efficient Solution Algorithms for the Riemann Problem for Real Gases, *J. Comp. Phys.*, **59**, pp.264-289, (1985).

[7] P.L. ROE, Approximate Riemann Solvers, Parameter Vectors, and Difference Schemes, *J. Math. Anal. Appl.*, **38**, pp.640-658, (1982).

[8] F. DUBOIS, Boundary Conditions and the Osher Scheme for the Euler Equations of Gas Dynamics, Report No. 170, Centre de Mathématiques Appliquées de l'Ecole Polytechnique, (1987).

[9] R. ABGRALL, Généralisation du solveur de Roe pour le calcul d'écoulements de mélanges de gaz parfaits concentrations variables, *La Recherche Aérospatiale,* (1988).

[10] R.N. SCHWARTZ, Z.I. SLAWSKY, K.F. HERZFELD, Calculation of Relaxation Times in Gases, *J. Chem. Phys.*, **20**, pp.1591-1601, (1952).

[11] F. THIVET, M.Y. PERRIN, S. CANDEL, A Non-Equilibrium Model for Hypersonic Flow, submitted to *Phys. Fluids,*(1990).

[12] C.E. TREANOR, P.V. MARRONE, Effect of Dissociation on the Rate of Vibrational Relaxation, *Phys. Fluids,* **5**, pp.1022-1026, (1962).

[13] P.V. MARRONE, C.E. TREANOR, Chemical Relaxation with Preferential Dissociation from Excited Vibrational Levels, *Phys. Fluids,* **6**, pp.1215-1221, (1963).

[14] R.J. KEE, J.A. MILLER, T.H. JEFFERSON, CHEMKIN : A General-Purpose, Problem-Independent, Transportable, Fortran Chemical Kinetics Code Package, Report No. SAND80-8003, Sandia National Laboratories, (1980).

[15] C. PARK, On the Convergence of Chemically Reacting Flows, AIAA Paper 85-0247, AIAA 23rd Aerospace Sciences Meeting, Jan. 14-17, (1985).

[16] J.A. DESIDERI, J. PERIAUX (Eds.), Proceedings of the INRIA-GAMNI Hypersonic Workshop, Antibes, France, 22-25 January 1990.

[17] K.L. WRAY, *J. Chem. Phys.*, **36**, pp.2597, (1962).

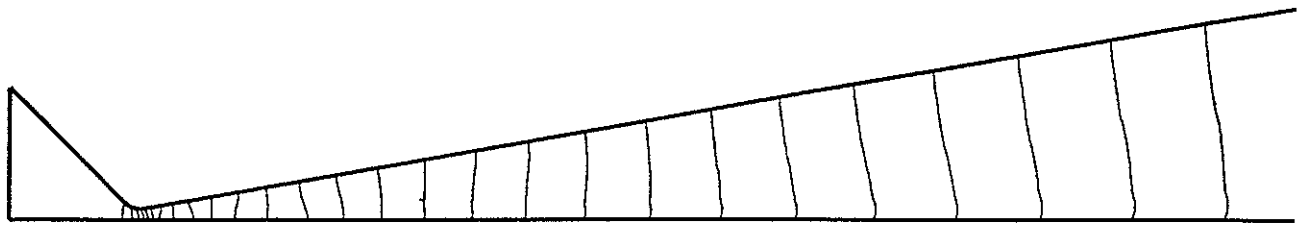

Figure 1: Frozen Mach Number. Min =4.197 10^{-3} ; Max = 11.93 .

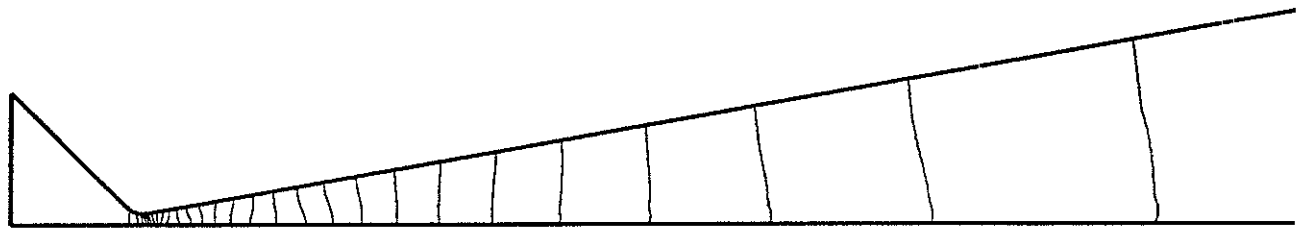

Figure 2: Trans-rotational Temperature. Min = 325.7 K; Max = 6494 K.

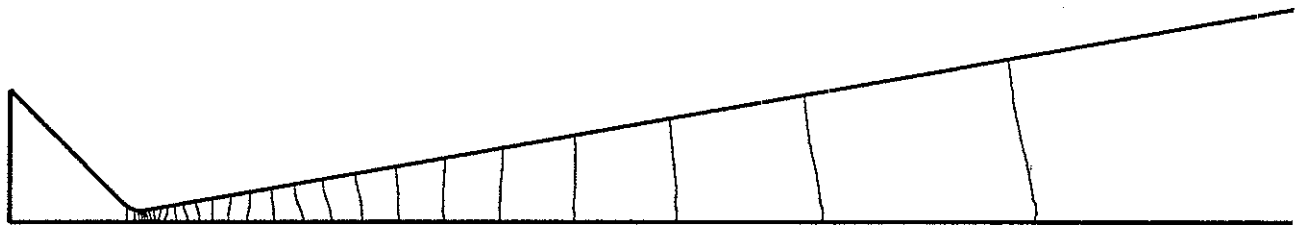

Figure 3: O_2 Vibrational Temperature. Min = 820.7 K; Max = 6494 K.

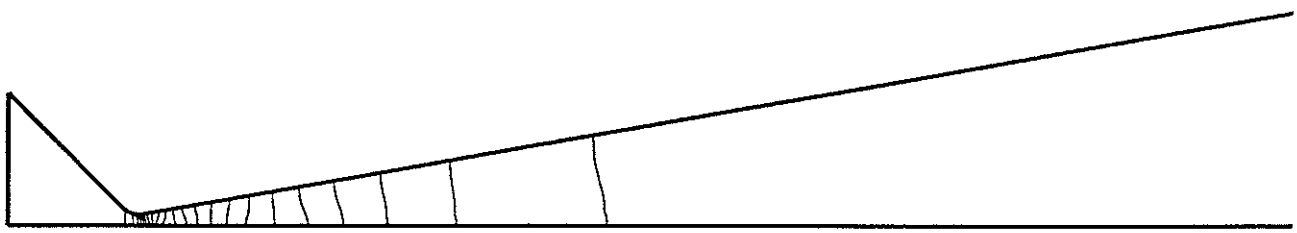

Figure 4: N_2 Vibrational Temperature. Min = 2063 K; Max = 6494 K.

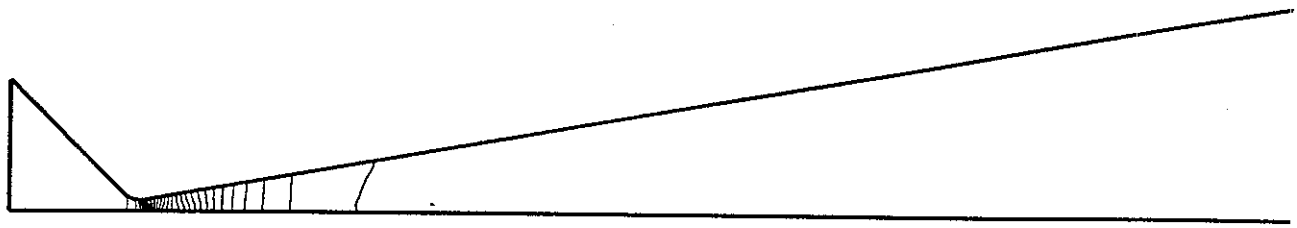

Figure 5: Mass Fraction of O_2. Min = 0.0481; Max = 0.1827.

Figure 6: Mass Fraction of N_2. Min = 0.6903; Max = 0.7341.

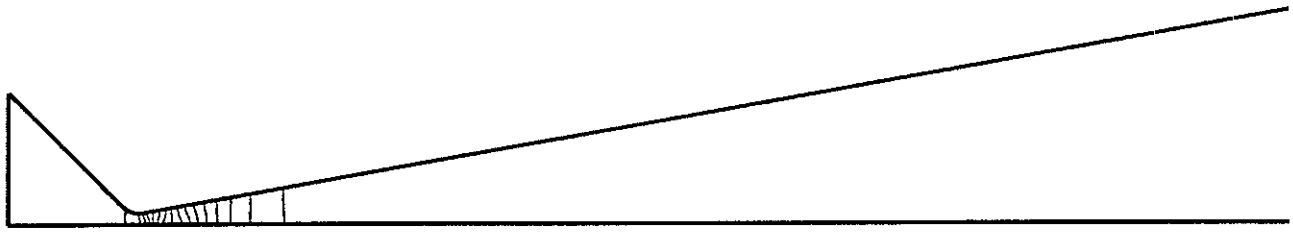

Figure 7: Mass Fraction of NO. Min = 0.07041; Max = 0.1509.

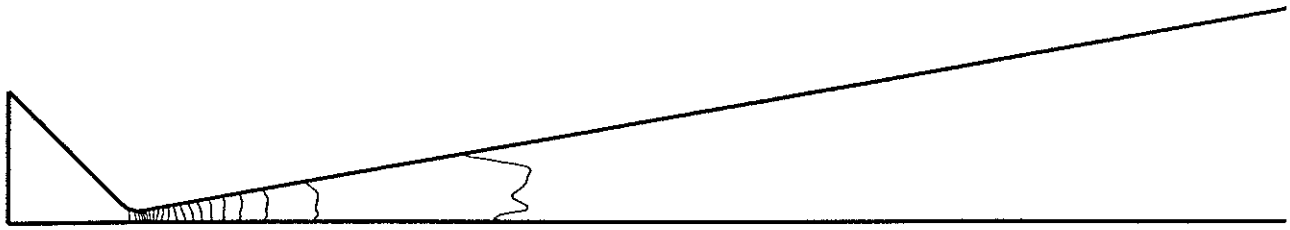

Figure 8: Specific Entropy. Δs = 20 J/K/Kg. Min = 1693; Max = 2135.

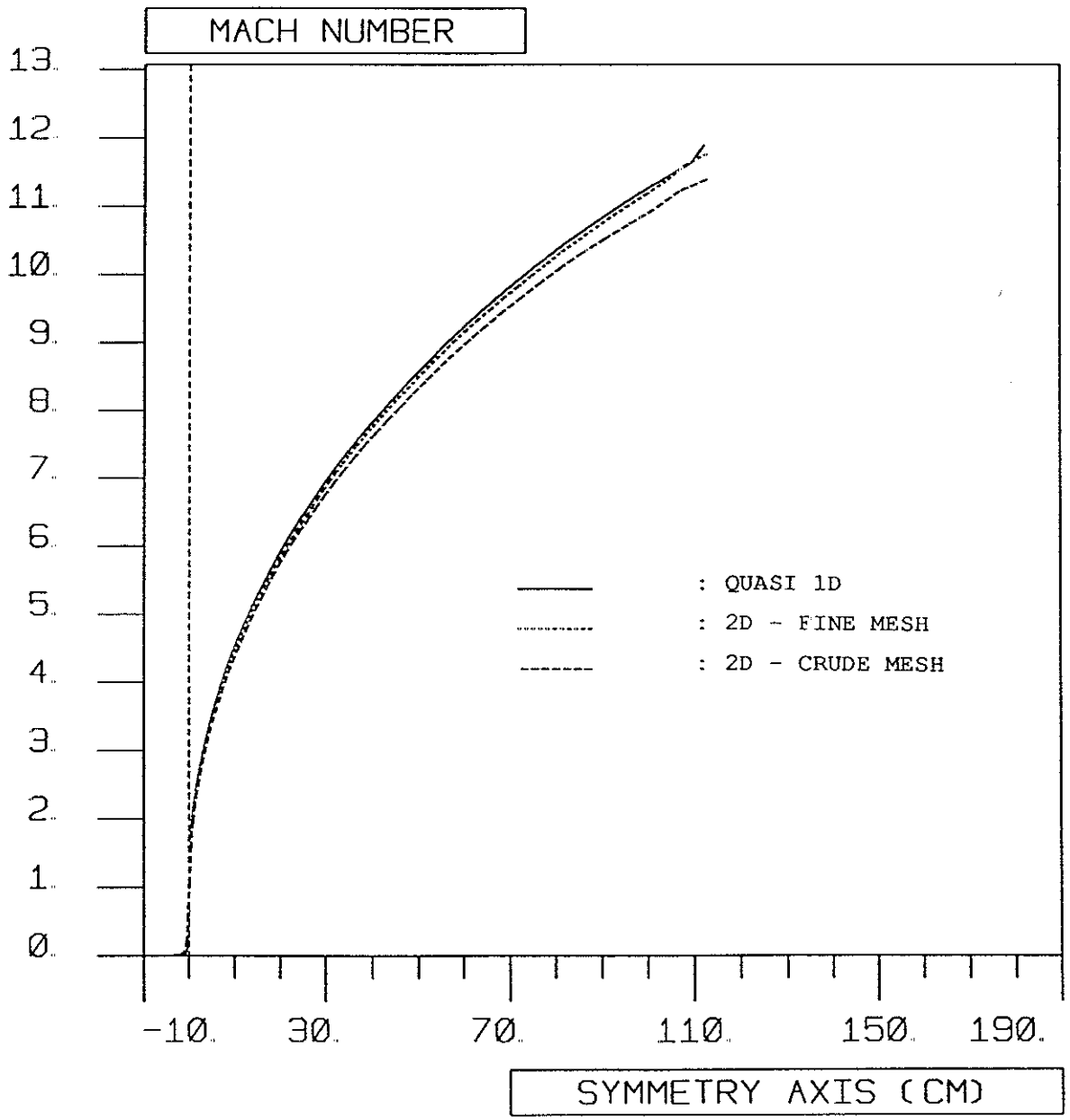

Figure 9: Frozen Mach Number.

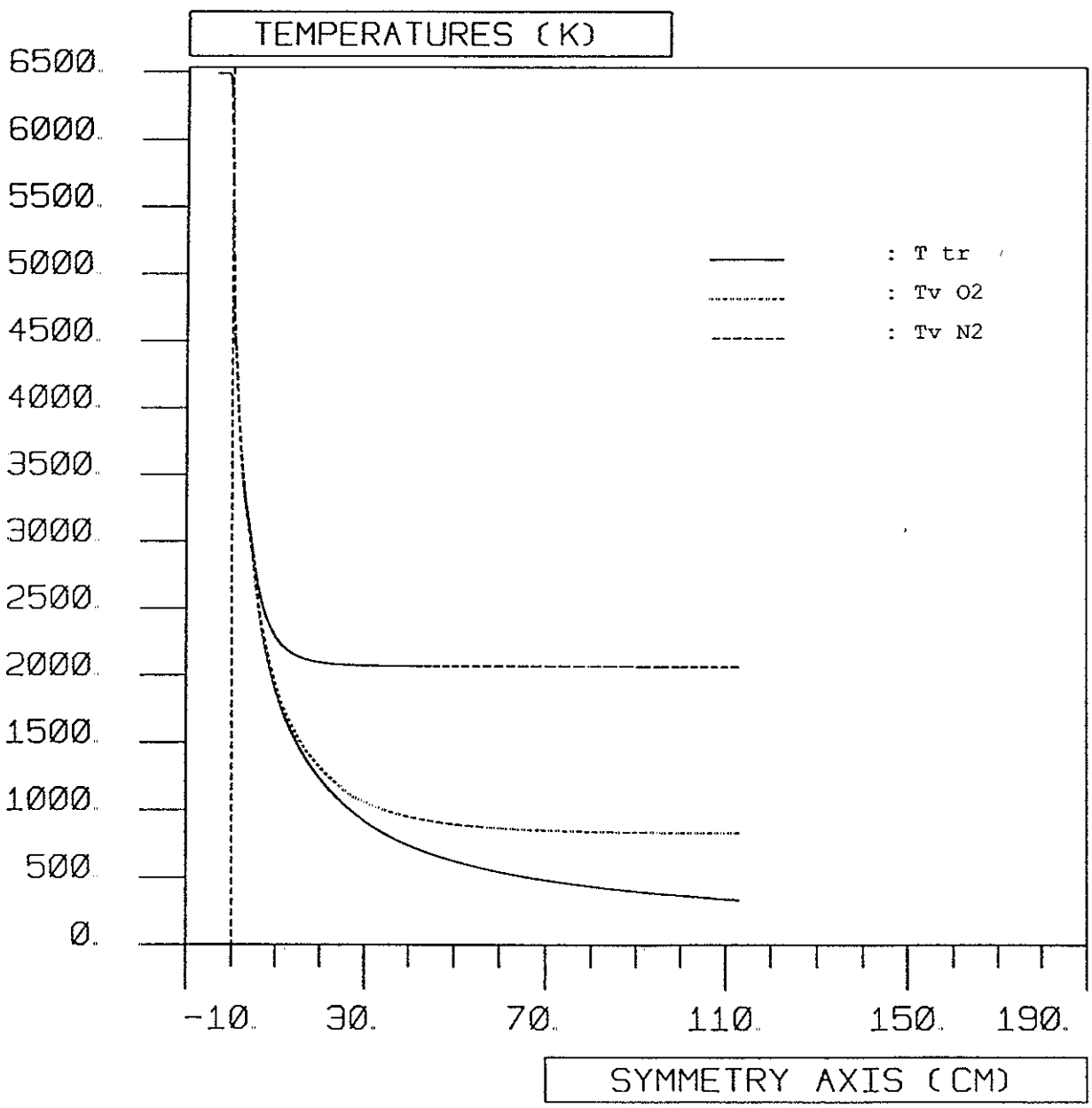

Figure 10: Temperatures.

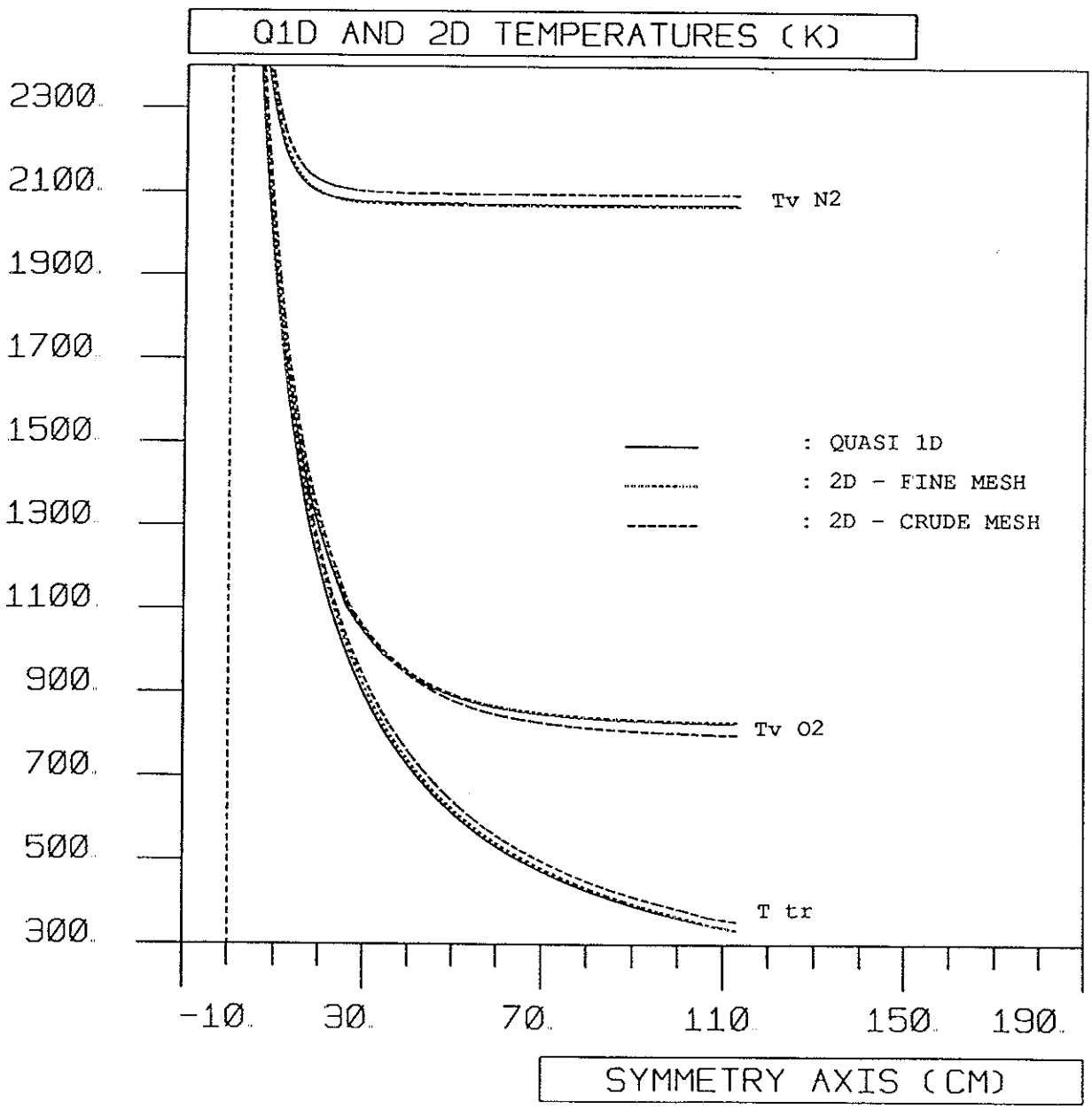

Figure 11: Comparison of Temperatures.

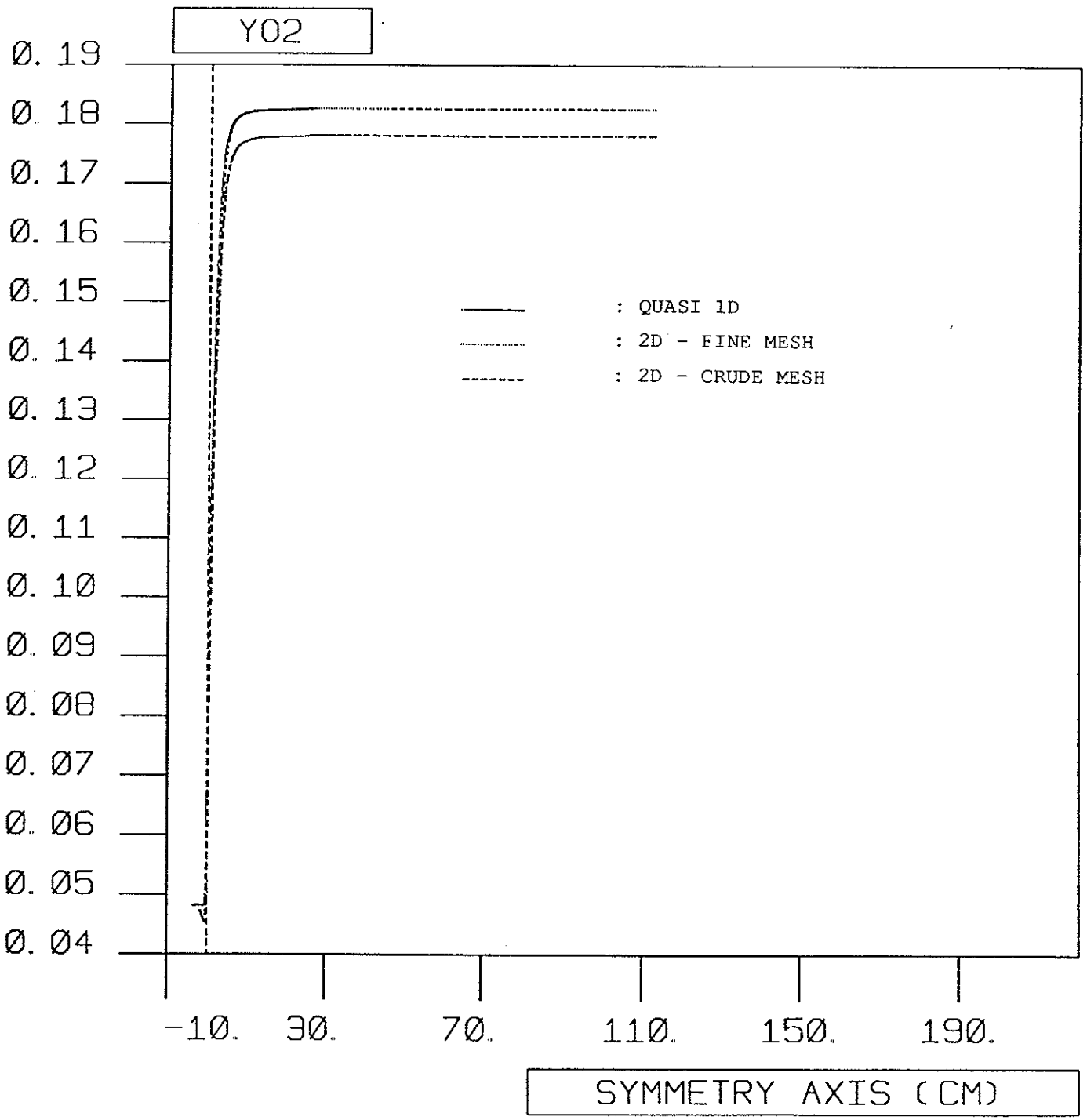

Figure 12: Mass Fraction of O_2.

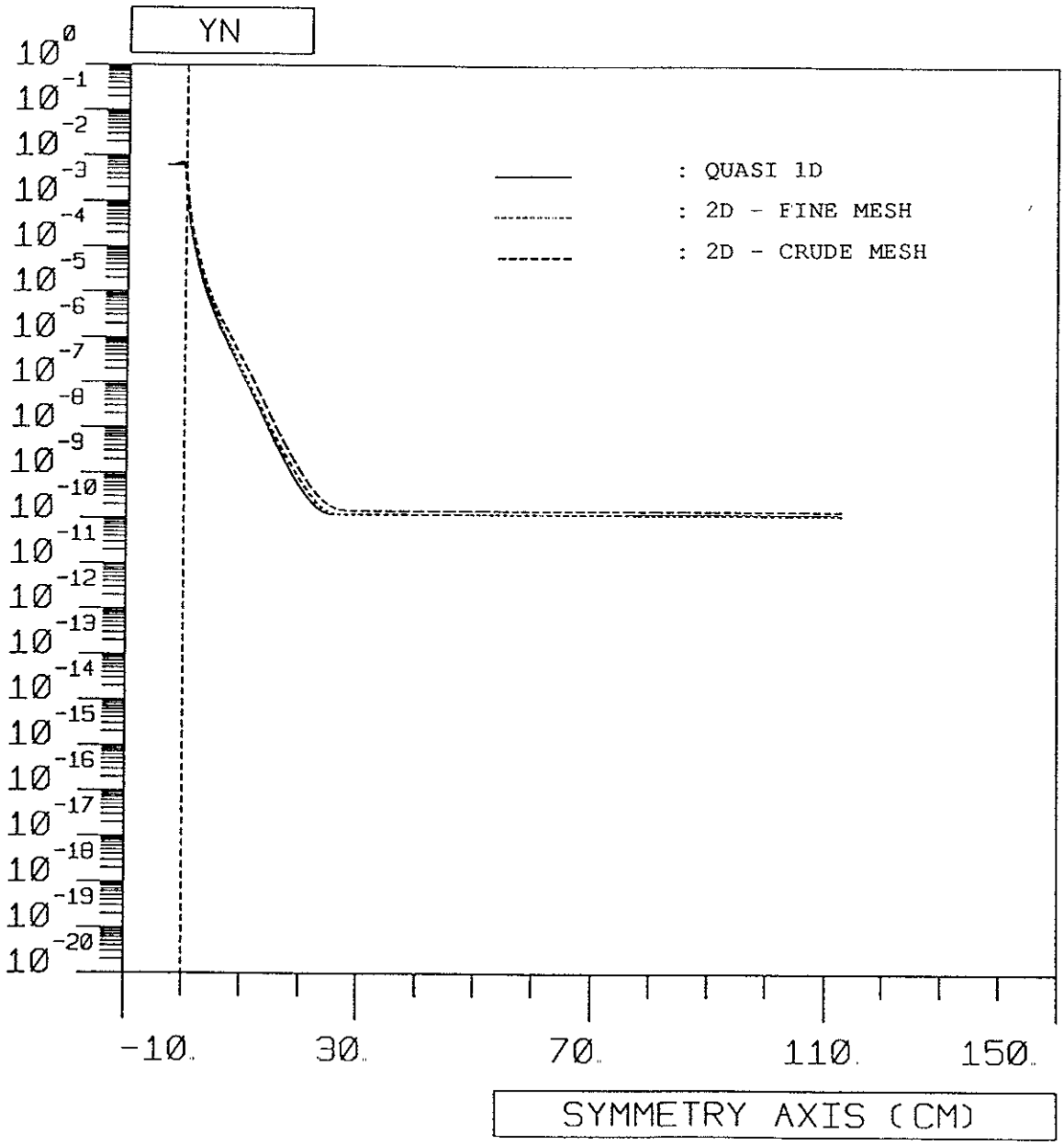

Figure 13: Mass Fraction of N_2

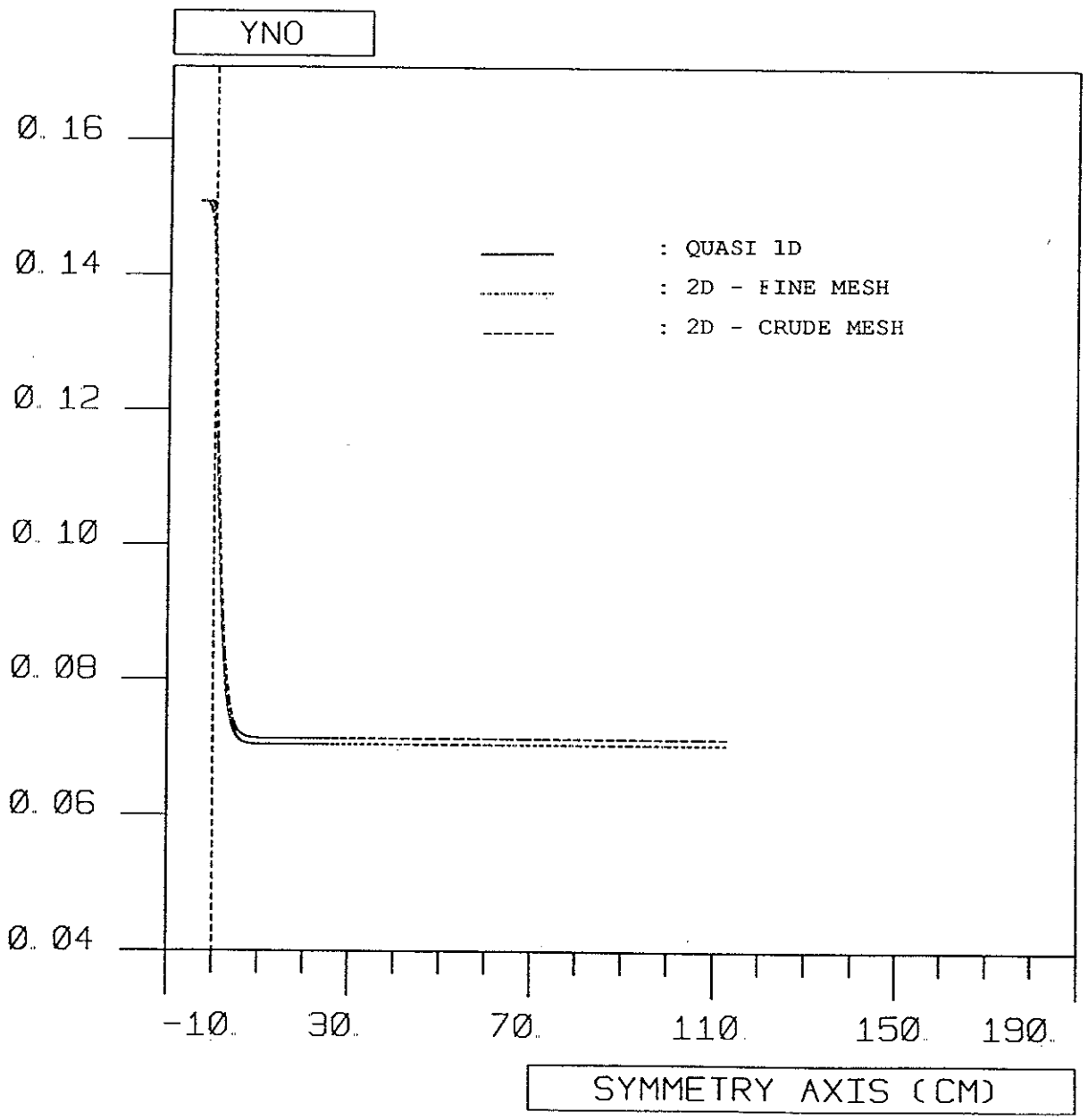

Figure 14: Mass Fraction of NO.

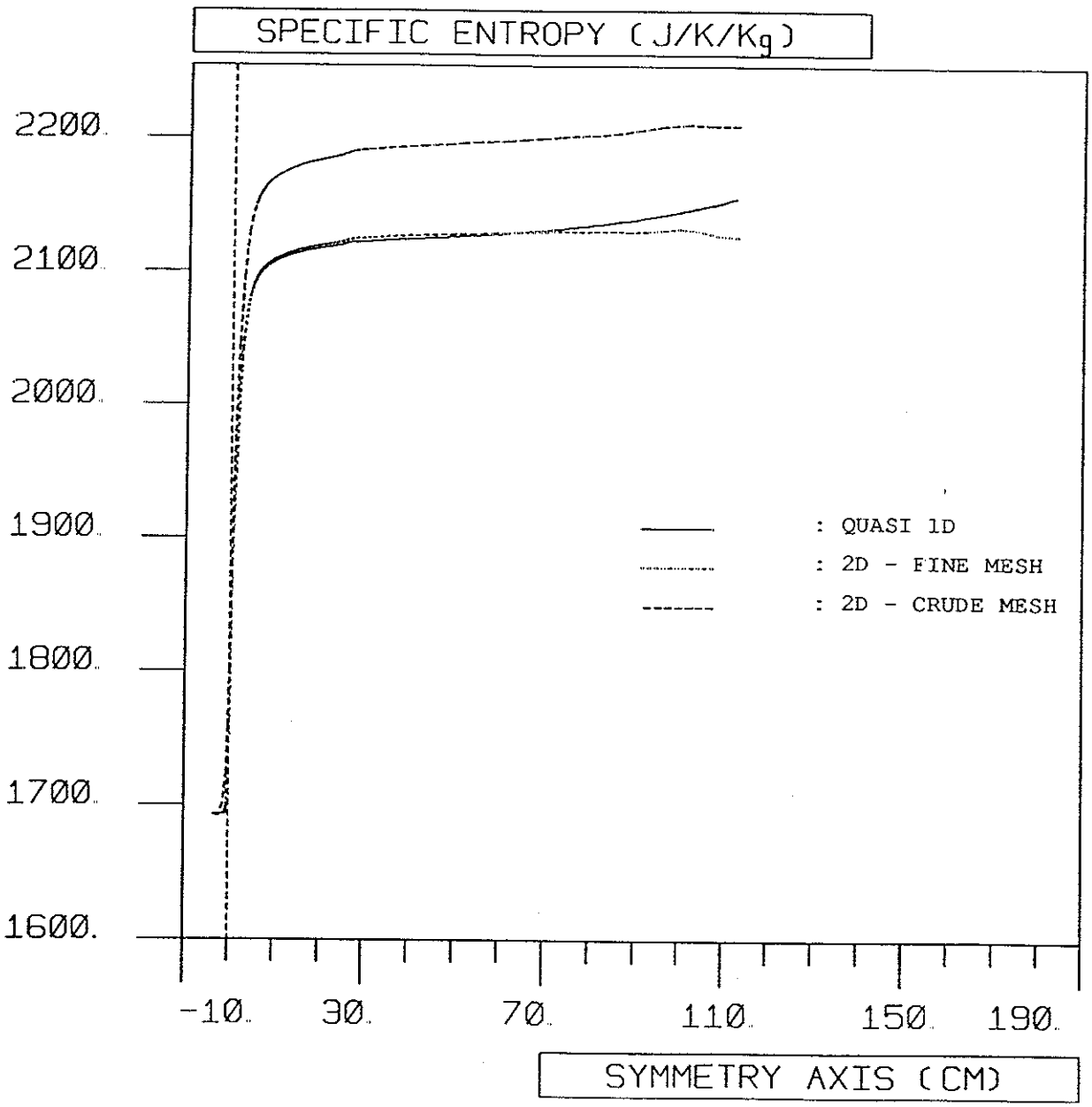

Figure 15: Specific Entropy. $\Delta s = 500$ J/K/Kg is represented by 1 cm.

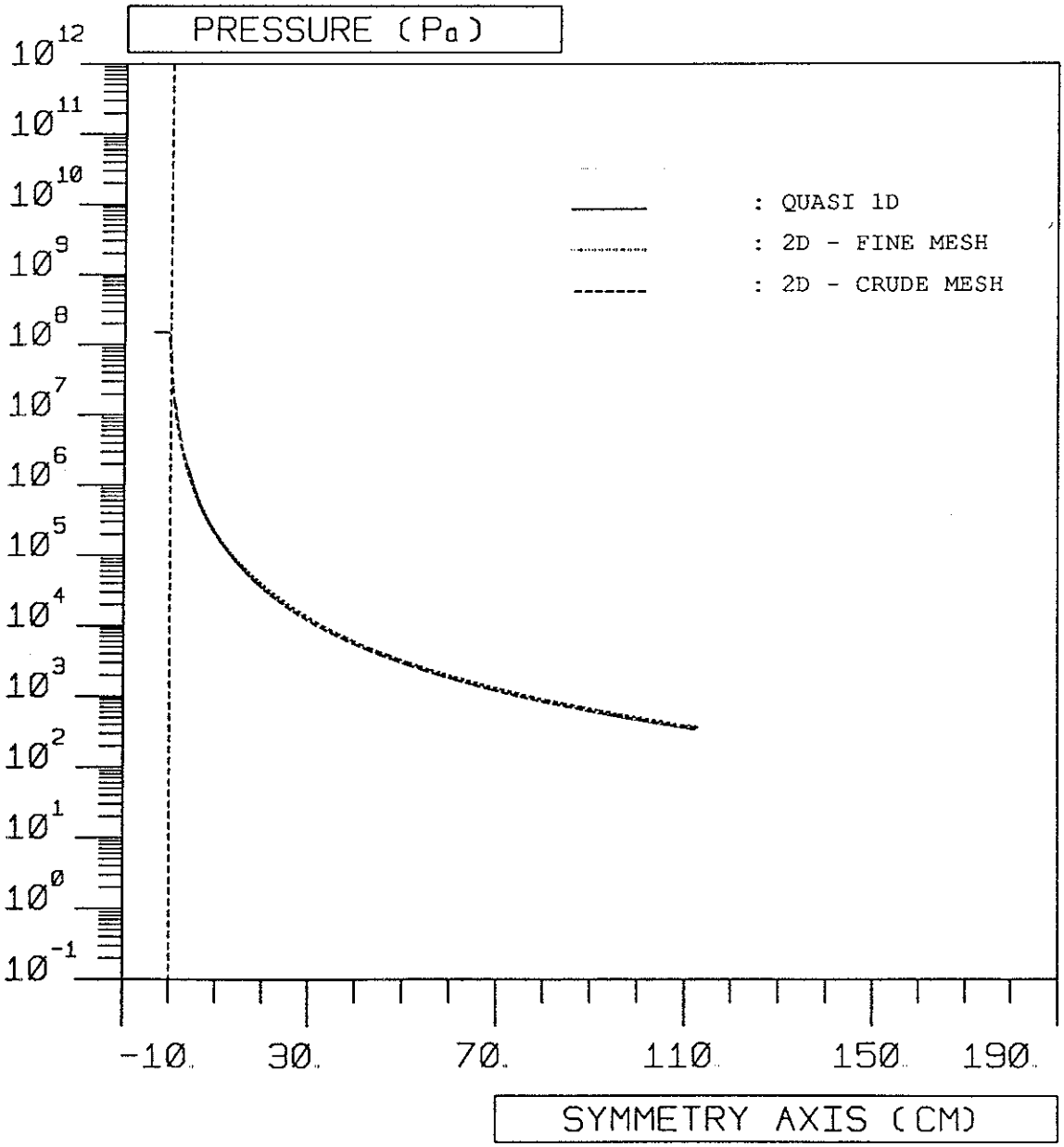

Figure 16: Pressure.

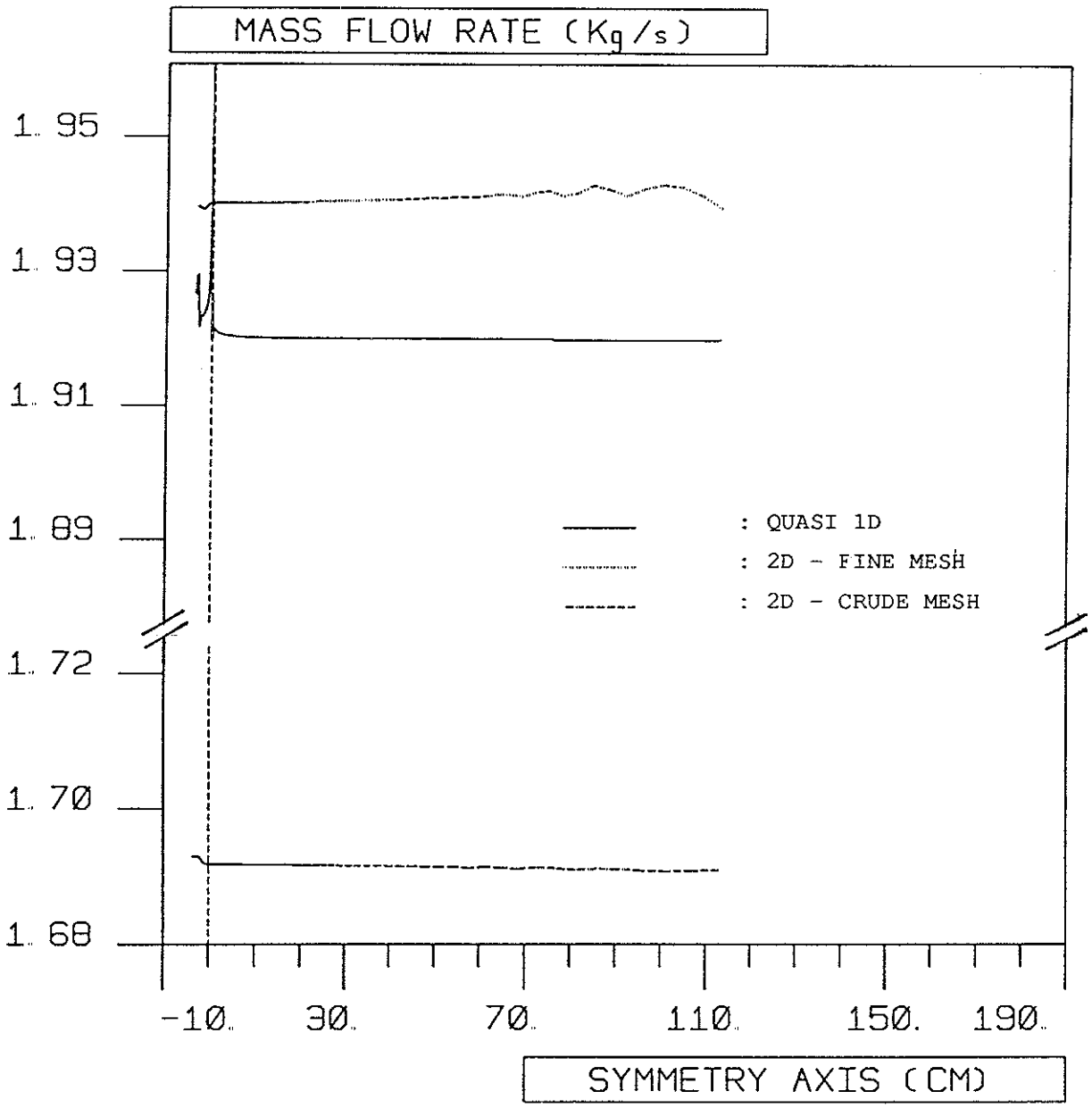

Figure 17: Mass Flow rate.

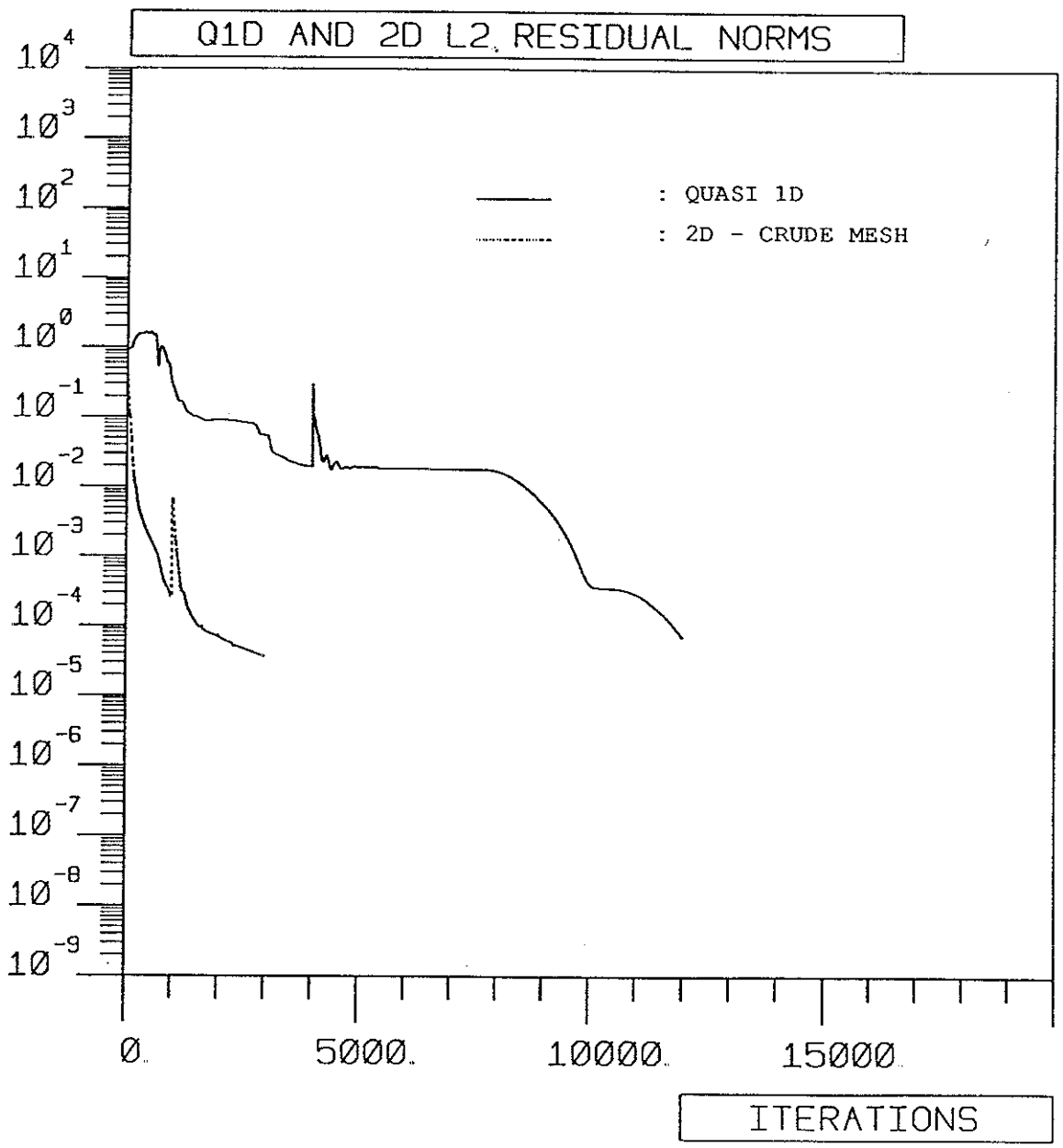

Figure 18: L_2 Norm of the residuals versus number of iterations.